

Plasmons and the spectral function of graphene

Marco Polini,^{1,*} Reza Asgari,² Giovanni Borghi,¹ Yafis Barlas,³ T. Pereg-Barnea,³ and A. H. MacDonald³

¹*NEST-CNR-INFM and Scuola Normale Superiore, I-56126 Pisa, Italy*

²*School of Physics, Institute for Studies in Theoretical Physics and Mathematics, 19395-5531 Tehran, Iran*

³*Department of Physics, The University of Texas at Austin, Austin, Texas 78712, USA*

(Received 28 July 2007; published 29 February 2008)

We report a theoretical study of the influence of electron-electron interactions on the one-particle Green's function of a doped graphene sheet based on the random-phase approximation and on graphene's massless Dirac equation continuum model. We find that states near the Dirac point interact strongly with plasmons with a characteristic frequency ω_{pl}^* that scales with the sheet's Fermi energy and depends on its interaction coupling constant α_{gr} , partially explaining prominent features of recent angle-resolved photoemission spectroscopy data.

DOI: [10.1103/PhysRevB.77.081411](https://doi.org/10.1103/PhysRevB.77.081411)

PACS number(s): 79.60.-i, 72.10.-d, 73.21.-b, 73.50.Fq

INTRODUCTION

The single-particle spectral function¹ $\mathcal{A}(\mathbf{k}, \omega)$ captures the influence of Coulomb and phonon-mediated interactions on the energy band properties of crystals. In this Rapid Communication we report a random-phase-approximation (RPA) theory of $\mathcal{A}(\mathbf{k}, \omega)$ in two-dimensional (2D) honeycomb-lattice carbon crystals described by their Dirac equation continuum model.^{2,3} Graphene sheets have attracted^{4,5} attention recently because of unusual properties that follow from their chiral band states, notably unusual quantum Hall effects,⁶ and because of their potential for technological applications. We find that states near the Dirac point ($\mathbf{k}=0$) of a graphene sheet interact strongly with plasmons with a characteristic frequency ω_{pl}^* that scales with the sheet's Fermi energy and depends on its interaction coupling constant α_{gr} , producing plasmonic spectral function satellites. The resulting⁷ spectral functions, illustrated in Fig. 1, have a broad energy spread near the Dirac point and a gap between the extrapolations of right-handed and left-handed bands to $\mathbf{k}=0$. We explain below why the Dirac point is special, even when it is not at the Fermi energy.

Angle-resolved photoemission spectroscopy (ARPES) is a powerful probe of $\mathcal{A}(\mathbf{k}, \omega)$ in 2D crystals because it achieves momentum \mathbf{k} resolution.⁸ Two recent experiments^{9,10} have reported ARPES spectra for single-layer graphene samples prepared by graphitizing the surface of silicon carbide (SiC).¹¹ Although the data in Refs. 9 and 10 are similar, the physical interpretations of the experimental findings are very different. Reference 9 discusses the ARPES spectra in terms of electron-phonon¹² and electron-plasmon interactions, while Ref. 10 focuses mainly on the apparent band gap opening at the Dirac point. A gap at the Dirac point can be explained without electron-electron interactions by assuming strong inversion symmetry breaking in the graphene layer due to coupling with the SiC substrate. Our theoretical results appear to allow an intrinsic interpretation for this feature, although it is clear that present experimental data are still partially obscured by incompletely controlled interactions with the substrate and by sample inhomogeneity, which produces momentum space broadening.

The self-energy in a system of fermions can be separated into an exchange contribution due to interactions with occu-

ried states in the static Fermi sea, and a correlation contribution due to the sea's quantum fluctuations.¹ Graphene differs¹³ from the widely studied 2D systems in semiconductor quantum wells because its quasiparticles are chiral and because it is gapless and therefore has interband quantum fluctuations on the Fermi energy scale. In graphene, band eigenstate chirality endows exchange interactions with a new source of momentum dependence, which renormalizes the quasiparticle velocity and strongly influences the compressibility and the spin susceptibility.¹⁴⁻¹⁶

DOPED DIRAC SEA CHARGE FLUCTUATIONS

The massless Dirac band Hamiltonian of graphene can be written as⁵ ($\hbar=1$) $\mathcal{H}=v\tau(\sigma_1 p_1 + \sigma_2 p_2)$, where $\tau=\pm 1$ for the inequivalent K and K' valleys at which π and π^* bands touch, p_i is an envelope function momentum operator, and σ_i

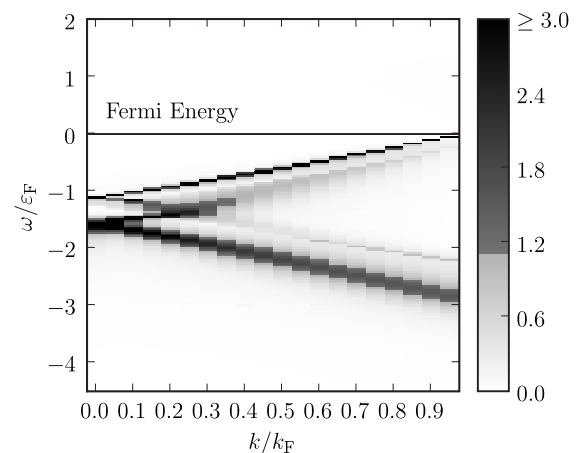


FIG. 1. Spectral function $\mathcal{A}(\mathbf{k}, \omega)$ of an n -doped graphene sheet as a function of k (in units of the Fermi wave vector k_F) and ω (in units of and measured from the Fermi energy $\hbar v k_F$ where v is the Fermi velocity). These results are for coupling constant $\alpha_{\text{gr}} = g e^2 / (\epsilon \hbar v) = 2$ (here $g=4$ is a spin-valley degeneracy factor and the dielectric constant ϵ depends on the material that surrounds the graphene layer). For each k ARPES detects the portion of the spectral function with $\omega < 0$. The k dependence is represented in this figure by results for 20 discrete $k \in [0.0, 0.95]$.

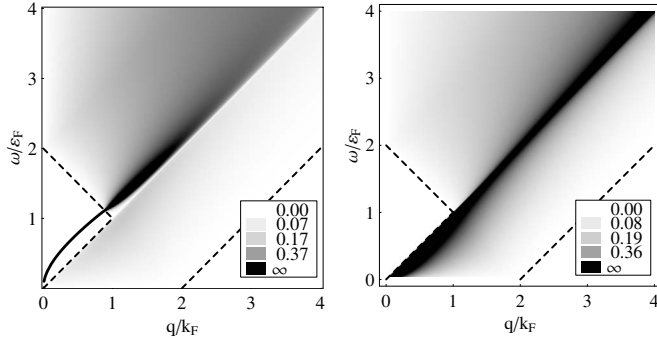


FIG. 2. Left panel: $\text{Im}[\varepsilon^{-1}(\mathbf{q}, \omega)]$ as a function of q/k_F and ω/ε_F for $\alpha_{\text{gr}}=2$. The solid line is the RPA plasmon dispersion relation. The dashed lines are the boundaries of the electron-hole continuum. Right panel: $v_q \text{Im}[\chi^{(0)}(\mathbf{q}, \omega)]$ as a function of q/k_F and ω/ε_F . The left and right panels become identical in the noninteracting $\alpha_{\text{gr}} \rightarrow 0$ limit.

is a Pauli matrix that acts on the sublattice pseudospin degree of freedom. The low-energy valence band states have pseudospin aligned with momentum, while the high-energy conduction band states, split by $2v|\mathbf{p}|$, are antialigned. In Fig. 2 we compare the particle-hole excitation spectra of noninteracting and interacting 2D doped Dirac systems. The noninteracting particle-hole continuum is represented here by the imaginary part of graphene's Lindhard function,^{15,17} $\text{Im}[\chi^{(0)}(\mathbf{q}, \omega)]$, which weights transitions by the strength of the density fluctuation to which they give rise. Transitions between states with opposite pseudospin orientation therefore have zero weight. More generally the band-chirality-related density-fluctuation weighting factor (called the chirality factor below), which plays a key role in the physics of the spectral function, is $[1 \pm \cos(\theta_{\mathbf{k}, \mathbf{k}+\mathbf{q}})]/2$ with the plus sign applying for intraband transitions and the minus sign applying for interband transitions, and $\theta_{\mathbf{k}, \mathbf{k}+\mathbf{q}}$ equal to the angle between the initial state (\mathbf{k}) and final state ($\mathbf{k}+\mathbf{q}$) momenta. The weight is therefore high for intraband (interband)

transitions when \mathbf{k} and $\mathbf{k}+\mathbf{q}$ are in the same (opposite) direction. The most important features in Fig. 2 are (i) the $1/\sqrt{vq-\omega}$ divergence which occurs near the upper limit of the $q < k_F$ intraband particle-hole continuum and (ii) the relatively weak weight at the lower limit of the $q < k_F$ interband particle-hole continuum. The divergence at the intraband particle-hole spectrum contrasts with the singular but finite $\sqrt{\omega_{\text{max}}-\omega}$ behavior at the upper end of the particle-hole continuum in an ordinary electron gas. The difference follows from the linear quasiparticle dispersion, which places the maximum intraband particle-hole excitation energy at vq for all k in the Dirac model case.

In the RPA, quasiparticles interact with Coulomb-coupled particle-hole excitations. Because the bare particle-hole excitations are more sharply bunched in energy, Coulomb coupling leads to plasmon excitations that are sharply defined out to larger wave vectors than in the ordinary electron gas and steal more spectral weight from the particle-hole continuum. As seen in Fig. 2, the plasmon excitation $\omega_{\text{pl}}(q)$ of the Dirac sea remains remarkably well defined even when it enters the interband particle-hole continuum. The persistence occurs because transitions near the bottom of the interband particle-hole continuum have nearly parallel \mathbf{k} and $\mathbf{k}+\mathbf{q}$ and therefore little charge-fluctuation weight. Interactions between quasiparticles and plasmons are stronger in the 2D massless Dirac system than in an ordinary parabolic-band 2D system.

DIRAC QUASIPARTICLE DECAY

In Fig. 3 we plot the imaginary part of the RPA theory¹ self-energy:

$$\text{Im}[\Sigma_s(\mathbf{k}, \omega)] = \sum_{s'} \int \frac{d^2\mathbf{q}}{(2\pi)^2} v_q \text{Im}\{\varepsilon^{-1}[\mathbf{q}, \omega - \xi_{s'}(\mathbf{k} + \mathbf{q})]\} \times \left(\frac{1 + ss' \cos(\theta_{\mathbf{k}, \mathbf{k}+\mathbf{q}})}{2} \right) [\Theta(\omega - \xi_{s'}(\mathbf{k} + \mathbf{q})) - \Theta(-\xi_{s'}(\mathbf{k} + \mathbf{q}))], \quad (1)$$

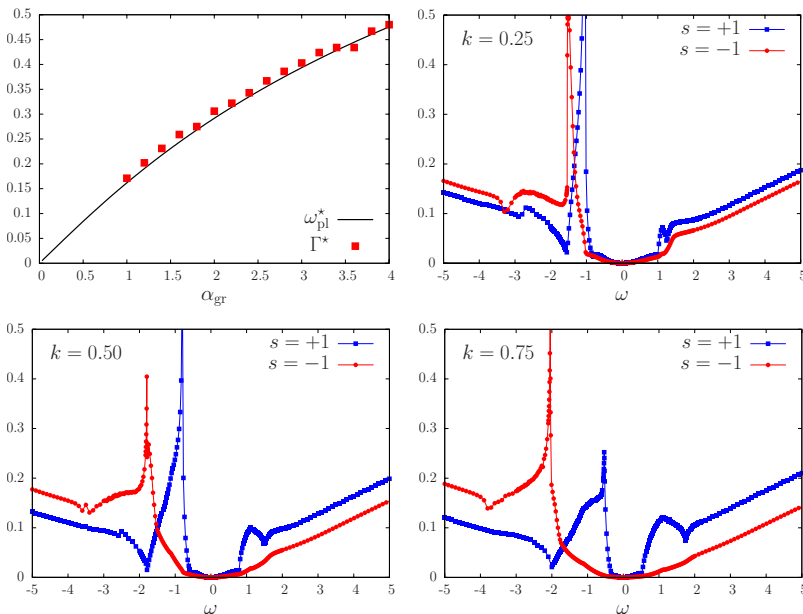


FIG. 3. (Color online) Top left panel: ω_{pl}^* (solid line) and Γ^* (filled squares) as functions of α_{gr} . Other panels: The absolute value $|\text{Im}[\Sigma_s(\mathbf{k}, \omega)]|$ of the imaginary part of the RPA quasiparticle self-energy (in units of ε_F) of an n -doped system as a function of energy ω for $k=0, 0.25$, and 0.75 and $\alpha_{\text{gr}}=2$.

where $s, s' = \pm 1$ are band (chiral) indices, $v_q = 2\pi e^2 / (\epsilon q)$ is the 2D Coulomb interaction, $\epsilon(\mathbf{q}, \omega) = 1 - v_q \chi^{(0)}(\mathbf{q}, \omega)$ is the RPA dielectric function, and $\Theta(x)$ is the Heaviside step function. $\text{Im}(\Sigma)$ measures the band-quasiparticle decay rate. The two factors in square brackets on the right-hand side of Eq. (1) express respectively the influence of chirality and Fermi statistics on the decay process. Note that Σ_s depends on the band index s only through the chirality factor. For $\omega > 0$ and fixed \mathbf{q} , the RPA decay process represents scattering of an electron from momentum \mathbf{k} and energy ω to $\mathbf{k} + \mathbf{q}$ and $\xi_{s'}(\mathbf{k} + \mathbf{q})$, with all energies in Eq. (1) measured from the Fermi energy. Since the Pauli exclusion principle requires that the final state be unoccupied, it must lie in the conduction band, i.e., $s' = +1$. Furthermore, since the Fermi sea is initially in its ground state, the quasiparticle must lower its energy, i.e., $\xi_{s'} < \omega$ —electrons decay by going down in energy. Because interaction and band energies in graphene's Dirac model both scale inversely with length, $\text{Im}[\Sigma_s(\mathbf{k}, \omega)] = vk_F F(\omega/vk_F, k/k_F)$. For large $|x|$, $F(x, y) \rightarrow -\pi \alpha_{\text{gr}}^2 \ell(\alpha_{\text{gr}}) |x| / (64g)$, where $\ell(0) = 4/3$ and $\ell(2) \approx 0.655$.¹⁸ This implies that for $|\omega| \gg vk_F$ the decay rate in a doped system $\{\text{Im}[\Sigma_s(\mathbf{k}, \omega)]\}$ approaches that of an undoped system. As we will see, however, doped-system properties are quite different from those of an undoped system up to energies several times larger than the Fermi energy, particularly so near the Dirac ($\mathbf{k} = 0$) point. The Fermi energy $\varepsilon_F = vk_F$ is used as the energy unit and k_F as the unit of wave vector in all plots and in the remaining sections of this Rapid Communication.

In explaining the spectra plotted in Fig. 3, we start with the Dirac point case for which the self-energy is band independent. For $\mathbf{k} = 0$, the final state energy $\xi_{s'}(\mathbf{q}) = s'q - 1$ is independent of the direction of \mathbf{q} . Because most charge fluctuation spectral weight is transferred from the particle-hole continuum to plasmonic excitations of the Dirac sea, $\text{Im}[\Sigma_s(0, \omega)]$ tends to be dominated by plasmon emission contributions. For $\omega > 0$ the final state must be unoccupied so that $s' = +1$; q is restricted to those values larger than 1 for which the Dirac sea excitation energy $\Omega(q) = \omega + 1 - q$ is positive. Comparing with Fig. 2, we see that $\text{Im}[\Sigma_+(0, \omega)]$ vanishes as ω^2 for $\omega \rightarrow 0$, a universal property of normal Fermi liquids.¹⁹ The sharp increase in $\text{Im}[\Sigma_+(0, \omega)]$ that occurs at $\omega \sim 1.2$ reflects the onset of plasmon emission. For $\omega < 0$ both conduction and valence band final states occur, and transitions are allowed if the transition energy $\Omega(q) = |\omega| - 1 + s'q$ is positive and the final hole state is occupied. Given ω , plasmon emission contributions occur when $\Omega(q) = \omega_{\text{pl}}(q)$ and are proportional to the plasmon spectral weight and to the density-of-states factor $|s' - d\omega_{\text{pl}}/dq|^{-1}$. The density-of-states factor is large for $s' = +$ and diverges when $\Omega(q)$ is tangent to $\omega_{\text{pl}}(q)$. The plasmon emission features in $\text{Im}[\Sigma_+(0, \omega)]$ are more prominent for holes than for electrons because this factor cannot diverge in the latter case. We find that $\text{Im}[\Sigma_s(0, \omega)] = -C\Theta(\omega + 1 + \omega_{\text{pl}}^*) \omega_{\text{pl}}^{*3/2} / \sqrt{\omega + 1 + \omega_{\text{pl}}^*}$ (with $C \sim 0.8$) near the decay peak. If we approximate this peak by a δ function, setting $\text{Im}[\Sigma_s(0, \omega)] \sim -\pi\Gamma^{*2} \delta(\omega + 1 + \omega_{\text{pl}}^*)$ and choosing the electron-plasmon coupling constant Γ^{*2} to reproduce the integrated strength of the feature over a ω_{pl}^* energy interval, we

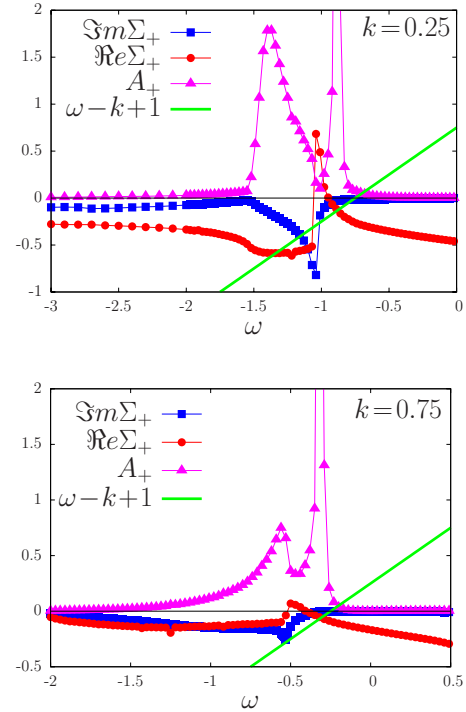


FIG. 4. (Color online) $\text{Re}[\Sigma_+(\mathbf{k}, \omega)]$, $\text{Im}[\Sigma_+(\mathbf{k}, \omega)]$, and spectral function $\mathcal{A}_+(\mathbf{k}, \omega)$ for $k=0.25$ and 0.75 . The band energy and $\text{Re}(\Sigma_+)$ are measured from the band ε_F and interaction $[\Sigma_+(k_F, \omega=0)]$ contributions to the chemical potential.

obtain a simple model in which a single band state hole with energy -1 interacts with a plasmon with energy ω_{pl}^* . Because Γ^* is comparable to ω_{pl}^* for all values of α_{gr} (see top left panel in Fig. 3) a significant part of the Dirac point spectral weight is always transferred to a plasmaron²⁰ satellite separated from the Dirac point band energy by $\sqrt{\omega_{\text{pl}}^{*2} + 4\Gamma^{*2}}$. This plasmaron satellite could be responsible for the broad photoemission spectrum^{9,10} at the Dirac point in epitaxial graphene samples if the sharper features present in Fig. 1 are obscured in current data by disorder-induced momentum space broadening. Away from the Dirac point, the conduction and valence band $\text{Im}[\Sigma_s(\mathbf{k}, \omega)]$ peaks broaden because of the dependence on scattering angle of $\xi_{s'}(\mathbf{k} + \mathbf{q})$, weakening any satellite features, and the plasmaron satellite fades. The $s=+$ and $-$ peaks in $\text{Im}[\Sigma_s]$ in Fig. 2 separate at finite k because of chirality factors which emphasize \mathbf{k} and \mathbf{q} in nearly parallel directions for conduction band states and \mathbf{k} and \mathbf{q} in nearly opposite directions for valence band states. The conduction band plasmon emission peak moves up in energy approximately as vk and the valence band peak moves down as seen in the bottom panels of Fig. 3.

SPECTRAL FUNCTION

ARPES measures the wave-vector-dependent quasiparticle spectral function.¹ Near the Fermi energy the spectral function consists of a narrow Lorentzian centered at the energy E which solves the Dyson equation for the $s=+$ quasiparticle energy, $E = \xi_+(\mathbf{k}) + \text{Re}[\Sigma_+(\mathbf{k}, E)]$. Near the Dirac point, the $s=+$ band spectrum separates into a quasiparticle

peak shifted to lower energies as explained above. In Fig. 4 we see explicitly that for $k=0.25$ there are already two solutions to the Dyson equation, although the largest part of the spectral weight still belongs to the quasiparticle peak. We also note in Fig. 4 that $\text{Re}(\Sigma_s)$ has a negative contribution that is present at the Fermi energy and persists over a wide regime of energy. This contribution is due to exchange and correlation interactions of quasiparticles near the Fermi energy with the negative energy sea. As explained previously,^{13,15,21} this effect produces a nearly rigid shift in the band energies that is increasingly negative further below the Fermi energy, increasing the band dispersion and the quasiparticle velocity. Figure 1 was constructed by combining results for $\mathcal{A}_s(\mathbf{k}, \omega)$ at 20 different values of $|\mathbf{k}|$ ($\mathcal{A}=\Sigma_s\mathcal{A}_s$). The plasmaron satellite in the $s=+$ band spectral function emerges gradually as $|\mathbf{k}|\rightarrow 0$. The $s=-$ band spectral function is identical to the $s=+$ band function at $|\mathbf{k}|=0$, but is substantially broader at larger $|\mathbf{k}|$ because of the large phase space for decay via particle-hole excitation further below the Fermi energy. The plasmaron satellite and the quasiparticle peak in the $s=-$ band tend to merge into one broad peak as $|\mathbf{k}|$ increases. The wave-vector-dependent exchange and correlation energy shifts discussed above also influence how the spectral function broadens at the lowest energies. It is abundantly clear that the spectral function of a doped system is similar to that of an undoped graphene system only for $k\gg k_F$.

Graphene ARPES spectra are influenced by disorder, coupling to the substrate, and electron-phonon interactions, in addition to the electron-electron interaction effects considered here. Because interactions effects scale with the vk_F energy scale, while phonon effects are fixed at optical phonon energy scales, these two contributions can be separated experimentally by varying the carrier density. Our RPA theory demonstrates that broad quasiparticle peaks and apparent energy gaps near the Dirac point are expected even without substrate coupling. We expect that the present RPA theory results, combined with progress in the preparation of samples suitable for ARPES or for 2D-to-2D tunneling spectroscopy,²² will enable further progress. We would also like to note that we recently became aware of related work by Hwang *et al.*²³

ACKNOWLEDGMENT

This work has been supported by the Welch Foundation, by the Natural Sciences and Engineering Research Council of Canada, by the Department of Energy under Grant No. DE-FG03-02ER45958, and by the National Science Foundation under Grant No. DMR-0606489. We thank T. Jungwirth, A. Lanzara, S. Louie, and A. Tomadin for helpful discussions.

*m.polini@sns.it

¹G. F. Giuliani and G. Vignale, *Quantum Theory of the Electron Liquid* (Cambridge University Press, Cambridge, U.K., 2005).

²K. S. Novoselov *et al.*, *Science* **306**, 666 (2004).

³T. Ando, T. Nakanishi, and R. Saito, *J. Phys. Soc. Jpn.* **67**, 2857 (1998).

⁴A. K. Geim and K. S. Novoselov, *Nat. Mater.* **6**, 183 (2007); M. I. Katnelson and K. S. Novoselov, *Solid State Commun.* **143**, 3 (2007).

⁵For a recent popular review, see A. K. Geim and A. H. MacDonald, *Phys. Today* **60**(8), 35 (2007).

⁶K. S. Novoselov *et al.*, *Nature (London)* **438**, 197 (2005); Y. B. Zhang *et al.*, *ibid.* **438**, 201 (2005).

⁷This information is available in numerical form upon request to the authors.

⁸A. Damascelli, Z. Hussain, and Z.-X. Shen, *Rev. Mod. Phys.* **75**, 473 (2003).

⁹A. Bostwick *et al.*, *Nat. Phys.* **3**, 36 (2007); *New J. Phys.* **9**, 385 (2007).

¹⁰S. Y. Zhou *et al.*, *Nat. Mater.* **6**, 770 (2007).

¹¹For a review, see W. A. de Heer *et al.*, *Solid State Commun.* **143**, 92 (2007).

¹²C.-H. Park, F. Giustino, M. L. Cohen, and S. G. Louie, *Phys. Rev. Lett.* **99**, 086804 (2007); W.-K. Tse and S. Das Sarma, *ibid.* **99**, 236802 (2007); M. Calandra and F. Mauri, *Phys. Rev. B* **76**, 205411 (2007).

¹³M. Polini *et al.*, *Solid State Commun.* **143**, 58 (2007).

¹⁴J. Gonzalez, F. Guinea, and M. A. H. Vozmediano, *Phys. Rev. B* **59**, R2474 (1999); M. I. Katnelson, *Eur. Phys. J. B* **52**, 151

(2006); D. V. Khveshchenko, *Phys. Rev. B* **74**, 161402(R)

(2006); E. G. Mishchenko, *Phys. Rev. Lett.* **98**, 216801 (2007);

O. Vafek, *ibid.* **98**, 216401 (2007); S. Das Sarma, E. H. Hwang,

and W.-K. Tse, *Phys. Rev. B* **75**, 121406(R) (2007); X.-Z. Yan

and C. S. Ting, *ibid.* **76**, 155401 (2007); D. E. Sheehy and J.

Schmalian, *Phys. Rev. Lett.* **99**, 226803 (2007).

¹⁵Y. Barlas, T. Pereg-Bernea, M. Polini, R. Asgari, and A. H. MacDonald, *Phys. Rev. Lett.* **98**, 236601 (2007).

¹⁶E. H. Hwang, Ben Yu-Kuang Hu, and S. Das Sarma, *Phys. Rev. B* **76**, 115434 (2007).

¹⁷See, e.g., B. Wunsch, T. Stauber, F. Sols, and F. Guinea, *New J. Phys.* **8**, 318 (2006).

¹⁸ $\ell(\alpha_{gr})$ has an analytical expression that is rather cumbersome and will be presented elsewhere.

¹⁹In the RPA we find $\text{Im}[\Sigma_s(0, \omega \rightarrow 0)] = -\sqrt{3}\alpha_{gr}^2\omega^2/[8g(1+\alpha_{gr})^2]$.

²⁰B. Lundqvist, *Phys. Kondens. Mater.* **6**, 193 (1967); L. Hedin *et al.*,

Solid State Commun. **5**, 237 (1967); S. M. Bose *et al.*, *Phys. Rev.*

Rev. **155**, 379 (1967); R. Jalabert and S. Das Sarma, *Phys. Rev.*

B **40**, 9723 (1989). An experimental observation of clear plas-

maron features in bismuth has been reported by R. Tediosi, N. P.

Armitage, E. Giannini, and D. van der Marel, *Phys. Rev. Lett.*

99, 016406 (2007).

²¹ $\text{Re}[\Sigma_s]$ is weakly dependent on the massless Dirac model's ultraviolet cutoff Λ (Refs. 13 and 15). The numerical results shown in this work have been calculated with $\Lambda=10^2$.

²²S. Q. Murphy, J. P. Eisenstein, L. N. Pfeiffer, and K. W. West, *Phys. Rev. B* **52**, 14825 (1995).

²³E. H. Hwang and S. Das Sarma, following paper, *Phys. Rev. B* **77**, 081412 (2008).